Ultraviolet camera measurements of passive and explosive sulphur dioxide emissions at Yasur volcano, Vanuatu

Ilanko, T.[1], Pering, T.D.[1*] Wilkes, T.C[1]., Woitischek, J.[2,3], D'Aleo, R.[4], Aiuppa, A[5]., McGonigle, A.J.S[1,6,7]., Edmonds, M[2]., Garaebaeti, E.[8]

[1] Department of Geography, University of Sheffield, Winter Street S10 2TN, UK
[2] Department of Earth Sciences, University of Cambridge, Downing Street CB2 3EN, UK
[3] BPI Institute, BP Institute, University of Cambridge, Madingley Rd, CB3 E0EZ, UK
[4] INGV, Sezione di Palermo, Via Ugo la Malfa 153, 90146, Palermo, Italy
[5] DiSTeM, Università di Palermo, Via Archirafi, 22, 90123 Palermo, Italy
[6] School of Geosciences, the University of Sydney, NSW2006, Australia
[7] Faculty of Health, Engineering and Sciences, University of Southern Queensland, Toowoomba, QLD 4350, Australia
[8] Geohazards Division, Vanuatu Meteorology and Geo-hazards Department, Lini Highway, Port Vila, Vanuatu

*Corresponding author: t.pering@sheffield.ac.uk

Abstract

Here, we present ultraviolet (UV) camera measurements of sulphur dioxide (SO_2) flux from Yasur volcano, Vanuatu, for the period 6th – 9th July 2018. Yasur commonly exhibits frequent strombolian explosions alongside persistent gas release. We use the 'PiCam' Raspberry Pi UV Cameras (Wilkes et al., 2017, 2016) but adapted for portability and powering through solar panels. Our determined median SO_2 fluxes range 4.0-5.1 kg s^{-1}, with maximum determined errors of -10.6% to +14.7%, including errors from gas cell calibration drift, plume direction and distance, and plume velocity. This work highlights the use of particle image velocimetry for the use of plume velocity determination, which was deemed preferable to typically used methods of cross-correlation and optical flow because of ability to operate across a range of plume conditions, and hence produced more reliable fluxes. We calculate SO_2 masses for strombolian explosions of 8 to 81 kg (mean of 32 kg) and through use of a simple statistical measure using the moving minimum we estimate that passive degassing is the dominant mode of degassing at Yasur averaging 69% of gas released. Our work serves to further highlight the utility of UV cameras measurements and the benefit of the multiple camera approach. Our work also adds to our inventory of gas-based data for strombolian explosions globally.

Highlights

- Long time series data collected using a portable solar chargeable UV cameras.
- Particle image velocimetry (PIV) used for plume velocity measurements.
- SO_2 fluxes range median values of 4.0-5.1 kg s^{-1}.
- SO_2 masses of strombolian explosions range 8 to 81 kg (mean 32 kg).

1. Introduction

Strombolian volcanism is one of the more common forms of basaltic explosive activity globally, associated with the rapid ejection of hot pyroclasts from a vent in a single impulsive event (Blackburn et al., 1976; Taddeucci et al., 2015), with event frequencies ranging from seconds to minutes (Pering and McGonigle, 2018). Volcanoes with frequent strombolian activity include: the archetypal Stromboli, Italy (Patrick et al., 2007; Ripepe et al., 2002); Pacaya, Guatemala (Battaglia et al., 2018; Dalton et al., 2010); Erebus, Antarctica (Johnson and Aster, 2005; Sawyer et al., 2011; Sweeney et al., 2008); and the subject of this study Yasur, Vanuatu (Bani and Lardy, 2007; Kremers et al., 2013; Oppenheimer et al., 2006). Other volcanoes also known to produce strombolian activity include: Etna, Italy (Aiuppa et al., 2016; Branca and Del Carlo, 2005; Pering et al., 2015) Villarrica, Chile (Shinohara and Witter, 2005); Arenal, Costa Rica (Garcés et al., 1998; Szramek et al., 2006); Batu Tara, Indonesia (Gaudin et al., 2017a; Laiolo et al., 2018); and Shishaldin, USA (Vergniolle et al., 2004).

Classically, this style of behaviour has been related to the ascent from depth of elongated and over-pressured bubbles, which expand in length rapidly towards the surface, termed gas slugs (Taylor bubbles) (Del Bello et al., 2012; James et al., 2008; Seyfried and Freundt, 2000; Taddeucci et al., 2015). However, recent research has suggested that causal mechanisms may be far more diverse (Barth et al., 2019; Suckale et al., 2016), and that the presence of crystal-rich layers in the magmatic column is important to the formation of a strombolian explosion. To test these hypotheses, it is useful to investigate the spectrum of strombolian activity at sites, such as Yasur, where it is typical. In addition, recent studies have highlighted the importance of eruption frequency in determining the behaviour of ascending gas slugs (Gaudin et al., 2017a) and their interaction for the classification of styles of behaviour into rapidly bursting slugs which may experience interaction with one another during ascent, through to single bursting slugs which do not interact (Pering et al., 2017; Pering and McGonigle, 2018)

There are several ways to obtain information about individual strombolian explosions, which could include seismic (Chouet et al., 2003; Ripepe et al., 2002), infrasonic (Dalton et al., 2010; Delle Donne et al., 2016; Johnson and Ripepe, 2011; Marchetti et al., 2009), thermal (Patrick et al., 2007; Ripepe et al., 2002), and gas-derived (McGonigle et al., 2009; Pering et al., 2015; Pering et al., 2016; Tamburello et al., 2012) data. Here, we focus on gas emissions using the ultraviolet (UV) camera, a frequently used technique for the measurement of gas release from persistently outgassing volcanoes (McGonigle et al., 2017; Pering et al., 2019a). The UV camera is able to resolve high-time resolution fluctuations in the release of sulphur dioxide (SO_2) emissions, and in tandem with a multi component gas analyser (Multi-GAS), which can measure gas ratios when placed inside a volcanic plume (Aiuppa et al., 2005; Shinohara et al., 2015), it is possible to estimate the total gas emissions (Pering et al., 2014). An important tool for understanding the mechanism for generation of strombolian explosions is the relative proportions of gas released during explosions and that released passively (Barth et al., 2019; Jaupart and Vergniolle, 1989, 1988; Parfitt, 2004; Suckale et al., 2016; Vergniolle and Jaupart, 1986). This ‘active’ to passive degassing ratio also provides information about conduit fluid dynamics (Gaudin et al., 2017a, 2017b; Pering et al., 2015; Pering et al., 2016). For example,

Tamburello et al., (2012) discovered that the most efficient mode of degassing at Stromboli was actually the passive degassing, which contributed to ~77% of gas release.

On determining gas mass from strombolian explosions (Mori and Burton, 2009; Pering et al., 2015; Tamburello et al., 2012), it is also possible, using gas ratios, to estimate total gas masses and volumes of events (Burton et al., 2007; Pering et al., 2016). These data can be applied to mathematical models, to glean further information about activity and generating mechanisms, including aspects such as slug length, explosive vigour, and categorising burst behaviour using fluid dynamics (Del Bello et al., 2012; James et al., 2009, 2008; Pering and McGonigle, 2018).

For this study we demonstrate the use of a very portable, solar-chargeable, version of the low-cost Raspberry Pi ultraviolet camera (Wilkes et al., 2017, 2016) combined with a new approach to plume velocity analysis for UV camera imagery to obtain sulphur dioxide fluxes. We illustrate the use of statistical methods to differentiate between passive and explosive gas release, and finally apply mathematical models to characterise the strombolian explosions at Yasur volcano.

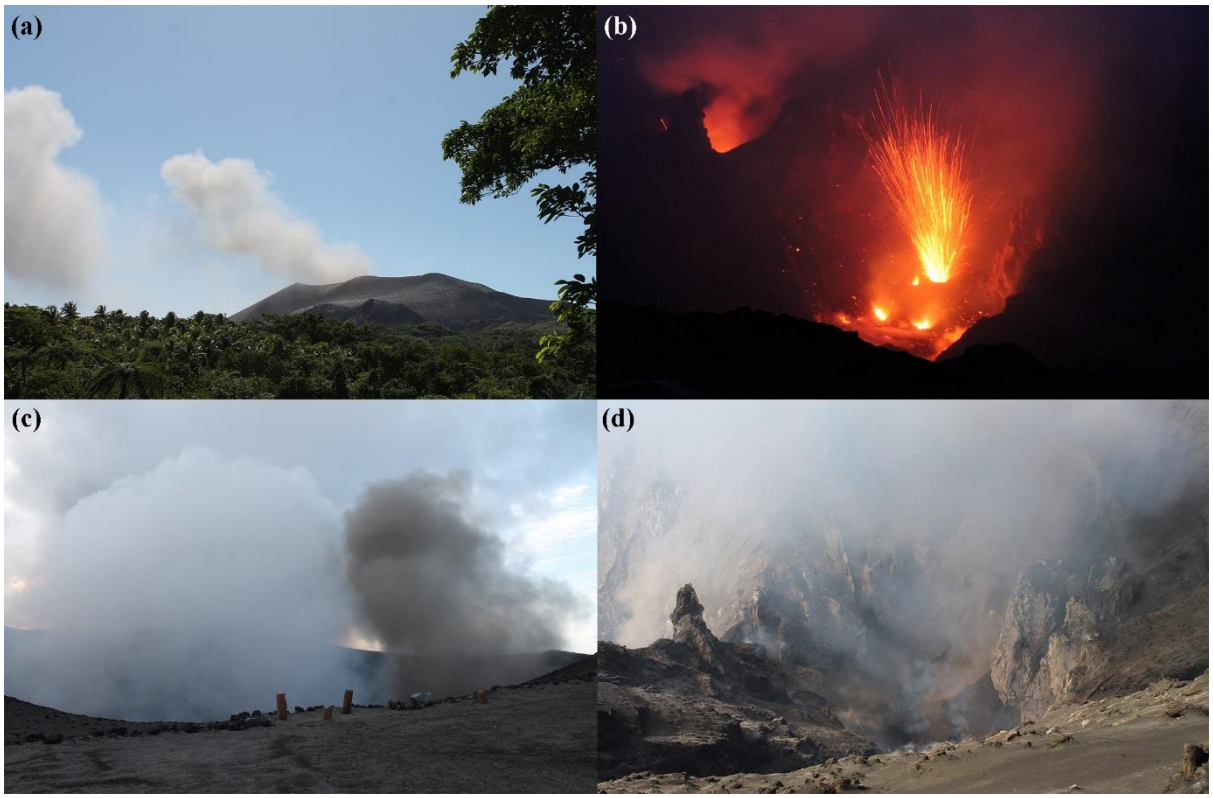

Figure 1: Example photos of activity during the field campaign. In (a) image of the gas plume from the summit crater, large pulses are associated with explosions; (b) a night-time view with the south crater in the foreground and incandescence of the north crater in the background, several vents are visible in the south crater with one in the process of a strombolian explosion; (c) the occasional contrast between the separate gas plumes of the ash-rich strombolian explosions from the north crater and the ash-poor plume and explosions from the south crater; (d) a day-time view into the north crater, with dividing boundary on the image left-hand-side.

2. Yasur volcano and activity during 5th-11th July 2018

Yasur is a basaltic volcano located on the southeast of Tanna Island, which is thought to have been predominantly persistently active for the last ~800-1400 years (Firth et al., 2014; Vergniolle and Métrich, 2016). The main volcanic edifice is a cone with a crater area of 350-450 m diameter, divided by a septum into northern and southern craters, each containing multiple active vents. During our period of measurement an ashy plume was present throughout the week, related to ash-rich strombolian explosions occurring from both craters (Figure 1). From the summit, multiple vents displaying incandescence were visible within the southern crater, each exhibiting different styles of explosive behaviour. Gas release from summit vents was constantly visible, occasionally including 'puffing' behaviour (Gaudin et al., 2017b, 2017a; Pering and McGonigle, 2018; Tamburello et al., 2012). The northern crater had at least two vents, but access to the northern crater rim was prevented by the frequency and location of ballistic impacts from strombolian explosions, which appeared to more ash-rich than those from the southern crater. From the southern crater we directly observed explosions from at least three vents, each exhibiting different characteristics, some with jet-like characteristics (i.e., rapid vertical movement in comparison to horizontal), highlight the potential for interaction with the conduit wall during the explosion process, i.e., the explosion (slug burst) happens within the conduit (Delle Donne and Ripepe, 2012). Another vent exhibited the parabolic transport of incandescent pyroclasts, as though an ascending bubble burst within an over-topped magma column (Del Bello et al., 2012) or within a flared geometry (Dibble et al., 2008). Interestingly these different styles of strombolian explosions also had clearly differentiable audible properties, with the latter associated with a deeper booming sound. During 8 – 9 July, explosions were frequently associated with visible shockwaves propagating through the condensed plume. Throughout the measurement period, the morphology of the crater was dynamic, with spatter and ash accumulating around vents leading to changes in the apparent size, shape, and position of vents.

A number of studies of Yasur have focused on the characteristics of strombolian activity and, in particular, its dynamism. Multi-vent basaltic volcanoes are known to exhibit vent-specific behaviours which can change through time, e.g., Salvatore et al. (2018) at Stromboli. Simons et al., (2020) discuss systematic changes in behaviour at individual vents within the southern crater at Yasur, with switching from bomb-rich (incandescent pyroclasts) through to ash-rich explosions. They also discuss conduit branching and a common source bubble (i.e., gas slug) for paired explosions from separate vents, with the potential for diverging eruption styles at the vents linked to cooling of the magma in the upper conduit. Spina et al., (2016), using infrasound, observed two distinct styles of degassing (puffing, which was observed as near-constant, and strombolian explosions), indicating that their behaviours were decoupled, while Meier et al., (2016) highlight the ash-rich and ash-poor (or bomb-rich) styles and their similarity to those of Stromboli (Gaudin et al., 2014b; Patrick et al., 2007; Ripepe et al., 2005; Ripepe and Marchetti, 2002; Taddeucci et al., 2012). Kremers et al. (2013) were able to calculate the lengths of gas slugs generating the strombolian explosions, ranging from 59 to 244 m, with a mean and median of 112 m and 103 m, respectively.

Regarding SO_2 fluxes, Bani and Lardy (2007), measured values ranging 2.5 to 17.2 kg s^{-1}, with a mean of 7.9 kg s^{-1} from April 2004 to November 2005 based on differential optical absorption spectroscopy (DOAS) traverses. Bani et al. (2012) published additional data collected between August 2007 and December 2008, with fluxes of 1.3 to 11.1 kg s^{-1}, with a mean and median of 7.2 kg s^{-1} and 7.1 kg s^{-1} respectively. Métrich et al., (2011) measured a mean of 8.0 ± 3.8 kg s^{-1} across four days of traverses in October 2007. Finally, Carn et al., (2017) show a satellite derived range of 6.8 to 23.3 kg s^{-1} measured between 2000-2015, with a mean and median of 16.3 kg s^{-1} and 19.2 kg s^{-1} ,respectively. With these values we emphasise the need to treat comparisons in gas flux between different periods of observations carefully, and that they may, in discrete campaigns such as presented in this study, not represent broader changes through time (or even match concurrent satellite derived estimates). Indeed, there are known issues when directly comparing satellite and ground-derived estimates of SO_2 outputs (Campion et al., 2012; McCormick et al., 2014).

3. UV Camera methods

Low-cost Raspberry Pi ultraviolet (UV) camera systems (the 'PiCam') were used, following (Wilkes et al., 2017, 2016); however, the PiCam had been modified to include 'PiJuice' hardware and software, attached to the Raspberry Pi board of each camera (https://github.com/PiSupply/PiJuice), i.e., there are two Raspberry Pi boards and PiJuice units per camera system. The PiJuice allows the continuous supply of power via mobile phone batteries, which can be recharged using solar panels. In the field, we used both 1600 mAh and 2300 mAh batteries and found that with continuous solar charging (using 40 W solar panels for each Pi board) these were effective in running the systems a day in the field. This camera setup also omitted the incorporated GPS module which automatically syncs time on Raspberry Pi start-up, instead opting to GPS sync time manually via the command line, which the PiJuice helps to regulate via a real-time-clock. Each camera system was equipped with two Edmund Optics Inc. filters (full width at half maximum of 10 nm), centred around 310 and 330 nm, one for each lens, to account for where SO_2 does and does not absorb UV radiation respectively.

Two separate camera systems (Camera 1 and Camera 2) were set up viewing the plume, southwest of the summit crater from a treehouse (Treehouse site, ~1900 m to plume) at the Jungle Oasis, on 6th and 7th July, and from the ash plain (Ash Plain site, ~2300 m to plume) to the north-northwest on 8th and 9th July (see Figure 2). The UV cameras were also operated on the 11th July; however, inclement weather and a grounding plume prevented reliable data processing. All times and dates are UTC. During measurement days, plume direction varied from west to northwest, with dry and predominantly cloud-free weather (bar a brief period of rain on the 9th July). Of the five days on which measurements were attempted, we acquired four days of high quality data, with over 16 hours collected across these days. We found it was possible to operate the cameras for 6–7 hours per day. From both locations, we had the opportunity to run both camera systems simultaneously. Images were acquired at acquisition rates of 0.5 – 0.25 Hz, with collection of clear images to account for vignetting and dark images for sensor noise, for each individual sequence. We conducted frequent calibrations using gas cells with known SO_2 concentrations (0 ppm, 412 ppm, and 1613 ppm; with a manufacturer

quoted error of 10 %) between measurement sequences, every 1-1.5 hours at a minimum, with additional calibrations when light conditions changed more rapidly. The data were then processed as per common protocols (D'Aleo et al., 2016; Kantzas et al., 2010; Kern et al., 2014; McGonigle et al., 2017) involving aligning images; selecting a clear sky background region; and choosing a plume cross-section along which to determine an integrated column amount (ICA), before multiplying by a plume speed to calculate flux. For flux data, we determined data normality statistically with the Kolmogorov-Smirnov normality test. The data were all non-normally distributed, therefore the median has been used in further calculations. However, we quote both mean and median values.

One of the goals of this study was to attempt to differentiate degassing form the vent areas. However, it was not possible to do this rigorously, or with enough confidence that we were resolving real differences in degassing, given that variable wind shear could lead to a separation of plumes or through crater derived eddying (Pering et al., 2019b; Tamburello et al., 2013), leading to incorrect identification. At times, the view from the ash plain site did allow us to identify gas pulses from separate sources, probably associated with explosions from the two craters (Figure 2c & d). Indeed, the plume predominantly appeared well-mixed on emergence from the summit crater. For example UV camera imagery see the supplementary video.

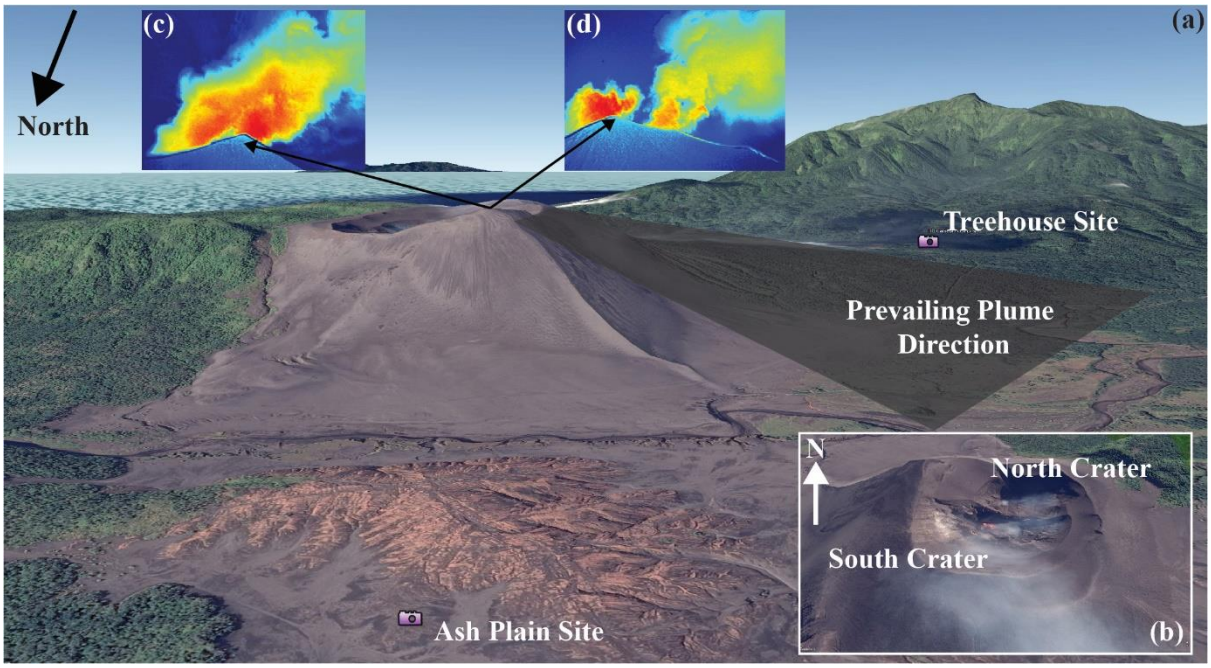

Figure 2: (a) An elevation-based perspective of the low summit of Yasur volcano, along with measurement positions and prevailing plume transport direction with inset (b) showing a close-up of the summit crater. In (c) a typical view of the plume with red colours representing higher concentrations of SO_2 with mixing between both crater areas, and (d) shows an example of where it was possible to differentiate between emissions from both craters. Imagery is from Google Earth®.

3.1. Particle Image Velocimetry (PIV) for plume velocity determination.

One of the most important, and yet potentially predominantly overlooked errors with UV camera analysis is with plume velocity determination, for which three main methods are commonly used: cross-correlation (McGonigle et al., 2005; Williams-Jones et al., 2006), optical-flow (Gliß et al., 2017; Kern et al., 2015; Peters et al., 2015; Peters and Oppenheimer, 2018), and manual tracking (Ilanko et al., 2019). Indeed, the exact method used will largely be determined by plume conditions, with no single method suited to all situations. Manual tracking can be good for stable plumes travelling at slow velocities, or for calculations at greater distances from the plume, which can be difficult to resolve using cross-correlation or optical-flow, as the plume is more dilute and fewer pixels containing SO_2 are available. Cross-correlation could be preferred on broadly homogenous plumes that are well-mixed and present little turbulence (e.g., SO_2 travelling backwards relative to the plume); and optical-flow may be better with similar high velocity plumes, where there may be differential velocities through pulsed gas outputs from craters, e.g., through strombolian explosions or puffing (Liu et al., 2019; Peters et al., 2015).

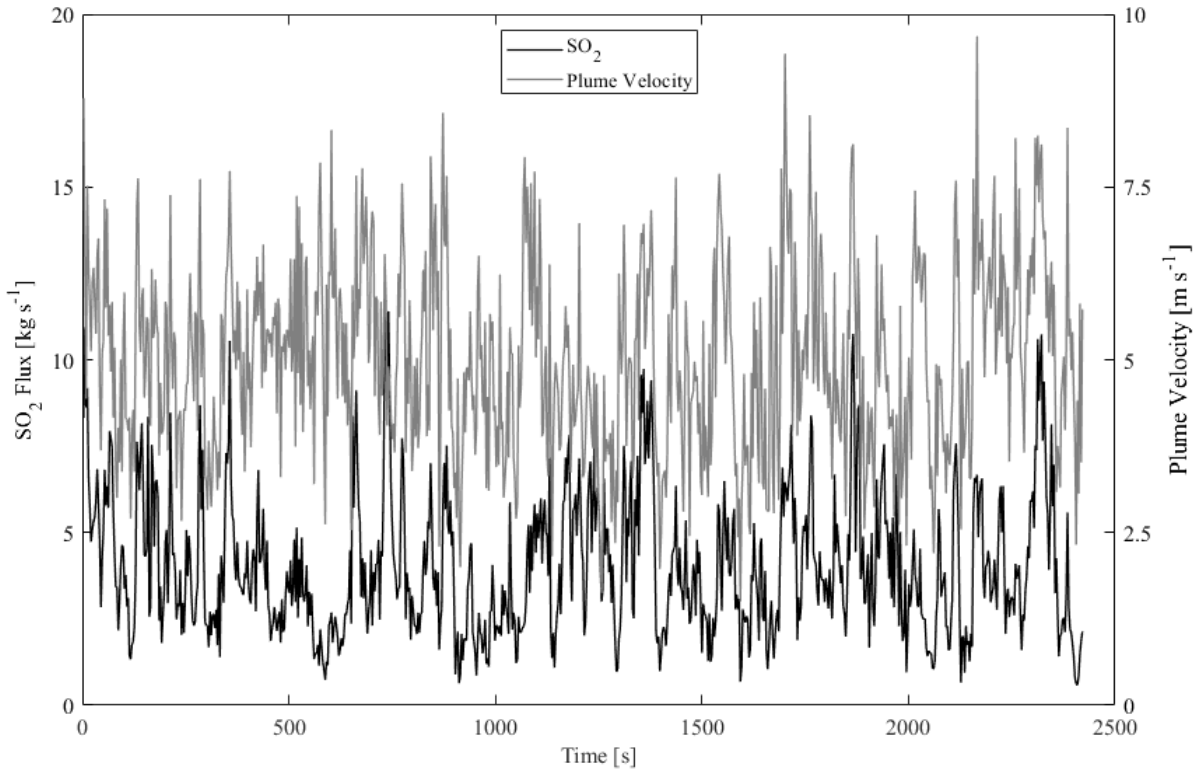

Figure 3: Example plume velocity and SO_2 fluxes for a period on the 7th July 2018, clear acceleration in plume velocities are evident, these occur during strombolian explosions.

Here, we encountered difficulties using these traditional methods, and needed a more efficient mechanism than manually tracking pulses of gas in such a large dataset. Indeed, cross-correlation sometimes failed, likely a result of turbulent motion in the plume, neglecting the fact that given visible increase in gas velocity (presumably following strombolian explosions), this method is probably the least favourable. Meanwhile, a lack of structure in the plume

appeared to lead to the failure of optical flow algorithms (Gliß et al., 2017; Peters et al., 2015; Wilkes et al., 2017). We therefore introduced the use of Particle Image Velocimetry (PIV) for plume velocity determination. Previous use of PIV in a volcanic context has included tracking of lava lake velocity at Masaya (Pering et al. 2019) and similar to the pyroclast tracking velocimetry of Gaudin et al. (2014a, 2014b). Here, we used PIVlab, a user-friendly MATLAB toolbox and app (Thielicke, 2014; Thielicke and Stamhuis, 2014). PIV works by comparing image pairs in sequences and looking for differences between them through two methods; direct cross-correlation or through the correlation of Fourier transforms. Both of these are conducted on integration areas (here we used three), with decreasing size on each pass. The end result is a velocity grid for the whole plume image, similar to those produced during optical flow (Gliß et al., 2017; Peters et al., 2015). We found that using PIV we were able to pick up velocity differences in more homogenous plumes (i.e., uniform SO_2 distribution through most of the plume, except during strombolian explosions). PIV was used to extract velocity components along the integration line, which could then be multiplied by the corresponding column amounts to yield our SO_2 fluxes (see Figure 3). The PIV analyses show temporal and spatial variability in plume speed, and this heterogeneity is not captured by cross-correlation or manual tracking. We report error for PIV analysis as the distance represented by each pixel divided by the lowest image capture frequency; for the ash plain this equates to an error of 2 ± 0.3 ms^{-1} or ~ ±15%, and for the treehouse site an error of 5 ± 0.6 ms^{-1} or ~9 ±%. These are based on typical plume speeds for each site.

3.2. Estimation of a total UV Camera Measurement Error

Error is an important aspect of all UV camera measurements. Here, we highlight the range of possible error sources, and perform additional analyses on our data related to calibration curve drift, plume orientation, and plume distance. The final determined values for error are our best possible estimate given the information and procedures conducted in-the-field, which, wherever possible, were designed to minimise error.

Campion et al., (2015) investigated the effects of light dilution at a range of volcanic targets and identified a broad range of ~10-60% underestimation in SO_2 content over a range of distances (2.1 km to 6.5 km) and conditions from hazy through to very clear. Light dilution will have a larger effect during hazier conditions, which were not present during our successful measurement days. Ilanko et al., (2019), calculated that at ~10.3 km distance (during clear conditions) SO_2 fluxes could be underestimated by 2.5 times, and at 4.25 km by 1.5 times (which would give ~1.18 times [18%] at our maximum distance of 2300 m). It is important to note that light dilution estimates are specific to each measurement location and given our range of distances to the plume and clear measurement conditions we suggest that error relating to light dilution is <+20%. We therefore take the value of +20% as our maximum light dilution error (i.e., light dilution causes underestimation). We also note that the plume was not optically thick, except following ash-rich strombolian explosions. Unfortunately, exact errors due to ash are currently not quantifiable, but we can state that ash within the plume will likely lead to an underestimation of values (Kern et al., 2013; Tamburello et al., 2012). We attempted to

minimise this error by integrating away from the summit area. We also further note that the peaks from strombolian explosions are well defined within the resulting dataset (Figure 3).

Table 1: A summary of error sources, values, including short comments and total RMS error.

	Treehouse	**Ash Plain**	**Comments**
Distance	1900 m	2300 m	-
Description	**Error**	**Error**	-
Light Dilution	+20%	+20%	Underestimation only, low given plume proximity.
Gas Cell Concentration	±10%	±10%	Manufacturer quoted
Calibration drift	+15%	+15%	Changing calibration conditions (see text)
Plume Velocity	±9	±15%	Based on pixel size (see text)
Plume Direction	±5%	±5%	Based on coincident UV camera data
Plume Distance	±18%	±18%	Based on plume deviation of 200 m.
Ash content	-	-	Underestimation, not quantifiable
RMS Error (Total)	-9.4% / +13.9%	-10.6% / +14.7%	Note the higher error related to underestimation (positive error).

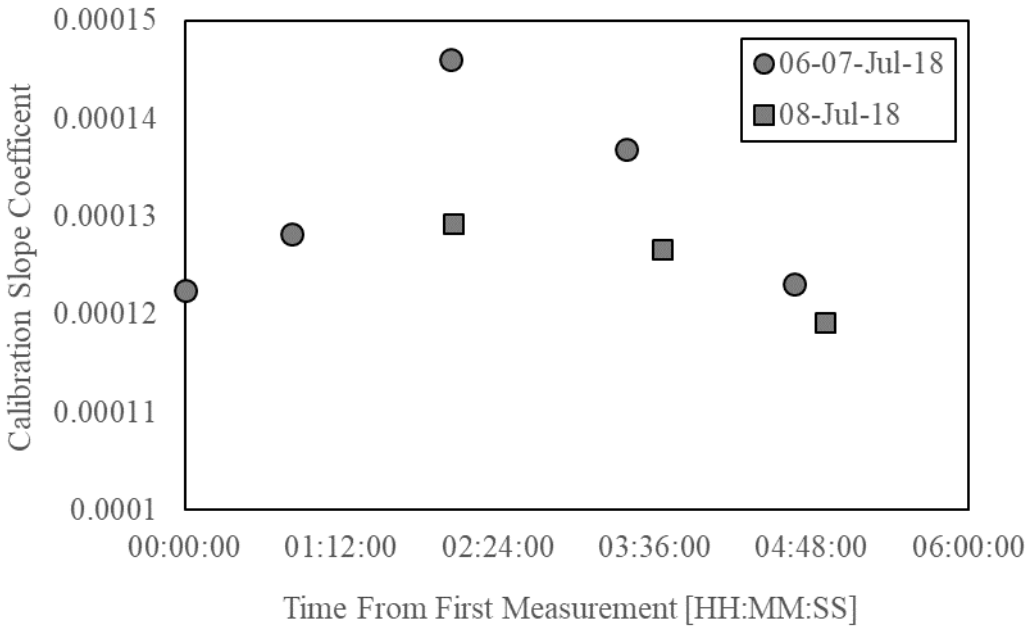

Figure 4: Example calibration slope coefficients from two days of data. Timings are from first calibration.

A gas cell calibration will alter throughout the day based on position of the sun and changing illumination as a result of background clouds, with gas-cell calibrations potentially over-estimating SO_2 column densities by up to 60% (Lübcke et al., 2013). Figure 4 shows the change in slope coefficient throughout the day from time of first calibration (rather than using UTC), varying from 1.22×10^{-4} to 1.46×10^{-4}. When taking into account the range in slope of 2.4×10^{-5}, and the broad assumption (for purposes of illustration) that there is linear change between

the first point and highest point (around the time of maximum solar height) we arrive, over 122 minutes, at a value of 1.97 x 10^{-7} increase in slope coefficient per minute. This would equate to a potential error of ~ 0.16% per minute, which expanded over an hour could become 9.6% - or, at our maximum calibration interval of ~95 minutes, an error of 15.2%. It is possible therefore that any underlying trends below these thresholds are not differentiable from this error, i.e., an increasing or decreasing flux at a rate of <~0.16% per minute. We suggest therefore that errors from cell calibration (notwithstanding the ~±10% manufacturer quoted cell content error) amount to a maximum of ~+15% for our measurement period.

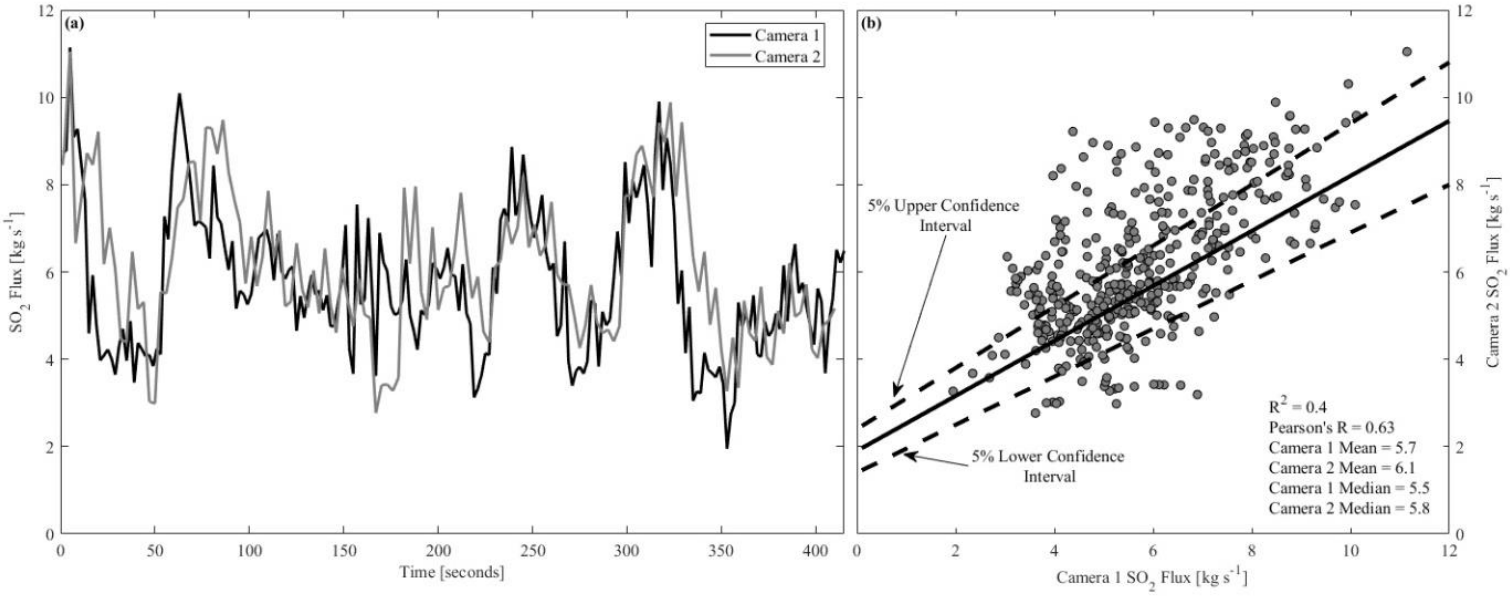

Figure 5: (a) Example period of overlapping data from two separately acquiring synchronous cameras at the same locations but with offset viewing angles. The data have been shifted by their maximum lag, determined using cross correlation. In (b) a linear regression model R^2 = 0.4 showing the best fit between data and confidence intervals. Statistical parameters are similar, but there are differences in peaks and troughs between the two datasets.

We used fixed distances of 1900 m and 2300 m from the camera to the plume for retrievals of data from the treehouse and ash plain sites respectively. For the ash plain data, we calculated that a 100 m error in plume distance leads to a < 5% difference in mass (with underestimation of distance corresponding to underestimation of mass), and a 200 m error in distance to < 9% error in mass. Comparisons of the same test dataset with different velocities in PIV analyses showed variations from 1 – 7 % with 100 m distance and 5 – 11% with 200 m distance. The combined effect of these distance errors on mass and velocity gives a 7-10% difference in fluxes for 100 m, and 16-18 % for 200 m. We therefore take the maximum value here of ~18% and apply this as a reasonable value for our entire dataset. As an example of how distance errors might affect our data, during the measurement period on 9th July the plume appeared to drift closer to the camera, which could have caused subsequent SO_2 fluxes to be underestimated.

Given changes in plume direction, the angle of the plume and where the integration line bisects the plume could also become important (Klein et al., 2017). To investigate this, we use overlaps

between data from two synchronously acquiring cameras (Figure 5), but with slightly different plume views and hence integration lines, simulating a potential difference from changing plume angle. Datasets were cross-correlated and shifted by lag indicated by maximum correlation to account for different transport times between integration lines. The calculated difference in flux retrieval, based on median values is ±5%. We note here that, there will be differences in arrival times and magnitudes of peaks and troughs in datasets based on smoothing or turbulence during plume movement through the atmosphere.

As an aside, we also include data on our final fluxes (Figure 6) during periods when the plume grounded and during heavy rainfall. During these periods, median SO_2 fluxes were underestimated by ~4.3-4.4 and 5.6-7.3 times, respectively, based on median values of measurements either side.

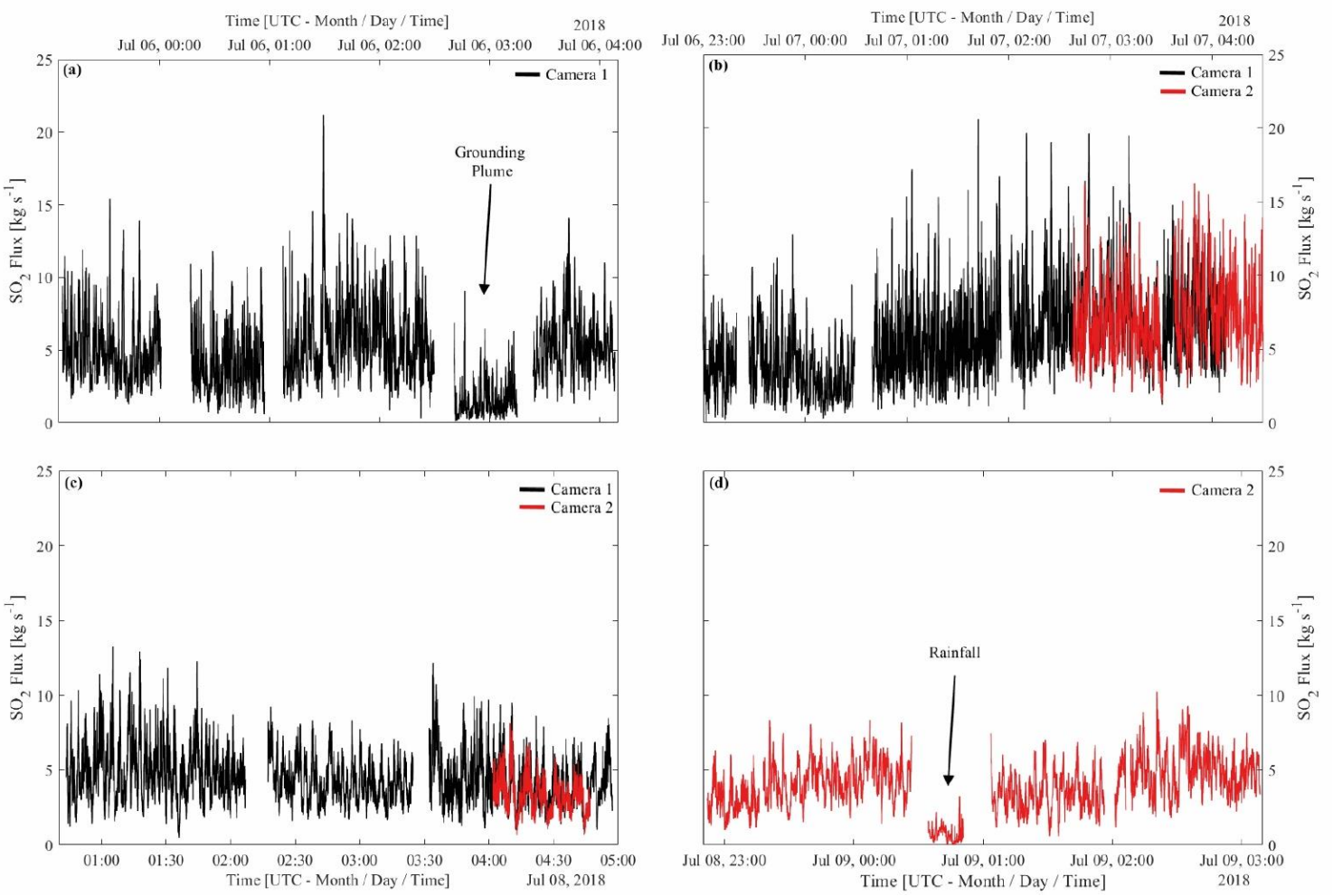

Figure 6: In (a) through (d) all measurement data during the observation period. Also highlighted are periods of grounding plume in (a) and rainfall in (d).

4. Results and Discussion

4.1 SO_2 Fluxes and Manually Derived Explosion Masses

Time series gas fluxes are shown in Figure 6, with a summary of daily statistics in Table 1. The median flux across the four days of measurements was 4.5 kg s^{-1} and the mean was 4.9 kg s^{-1}, reflecting the peaks in SO_2 flux associated with frequent strombolian explosions. This corresponds to a daily median and mean of 389 and 423 $t \cdot d^{-1}$. Daily statistics are given in Table 1: median SO_2 fluxes (calculated using the camera providing the bulk of each day's data) were between 4.0 – 5.1 kg s^{-1}. The means for each day were 4.1 to 5.5 kg s^{-1}. The timeseries data are suggestive of gradual changes in background gas release trends over several hours, but it is not clear whether these are real or a product of error. A shift in activity is, however, suggested by the observation of large strombolian explosions with visible ballistics and shockwaves, particularly on 8th and 9th July, when lower fluxes were measured.

Table 2. A summary of measurement durations and SO_2 flux statistics for our measurement period.

Date (UTC)	**05-06/07/18**	**06-07/07/18**	**08/07/18**	**08-09/07/18**
Time series duration (hh:mm)	4:15	04:42	03:54	03:33
Total time (hh:mm)	05:01	05:31	04:14	04:17
Mean (kg/s)	5.2	5.5	4.5	4.1
Median (kg/s)	4.7	5.1	4.2	4.0

Explosion masses were calculated following the method of Tamburello et al., (2012), by integrating beneath the explosive pulse and summing the total SO_2 released. Although, a key difference here is that strombolian explosions were not visible within the imagery (i.e., vents were at depth within the crater). We use two methods to determine explosion occurrence within the UV camera imagery, primarily when gas pulses in the camera images are seen to originate and visibly accelerate from the edge of the summit crater (see Figure 1a), but also where explosion traces show the characteristic coda detailed in Pering et al., (2016). Note here that there is therefore an underestimation in the number of explosions, however, their calculation is useful for comparison to literature values, and Table 3 shows a summary. Overall, we extracted SO_2 masses for 135 explosions, across the five UTC dates. We show an increasing mean mass from 6th to 9th July, which corresponds to visual observations of more powerful explosions on 8th and 9th July.

The range of SO_2 explosion masses at Yasur are in the range of 8 – 69 kg (mean 32 kg) and similar to those of Tamburello et al., (2012) at Stromboli with a range of 2 – 55 kg (mean of 20 kg); but higher than those at Etna during mild strombolian activity determined by Pering et al., (2015) on Etna, with a range of 0.1 – 14 kg. Woitischek et al., (In Review) present gas ratio data (SO_2, H_2S, H_2O and CO_2) derived from a combined Fourier transform infrared spectroscopy (FTIR) and Multi-GAS study, from a study period following our observations, with a brief overlap. The authors separated passive from explosive molar ratios, determining active (strombolian) ratios of: $CO_2/SO_2 = 2.85 \pm 0.17$; $H_2O/SO_2 = 315 \pm 71.8$; $SO_2/HCl = 1.6 \pm 0.22$. From these we can estimate total slug masses which are highlighted in Table 3. Our

mean total gas mass based on mean active ratios indicate a mean of ~2960 kg and range of 910 – 5940 kg for strombolian explosions at Yasur. These compare with a range of 170 – 1674 kg for Pacaya (Dalton et al., 2010); whilst at Stromboli values range 44 to 238 kg according to Barnie et al. (2015) and 2 to 1425 kg as determined by Delle Donne et al. (2016).

Table 3: A breakdown of data related to SO_2 explosion masses measured on a data by data basis. Also displayed are our passive to explosive percentages. Lower and Max ratios refer to the ranges indicated in determined active molar ratios by (Woitischek et al., In Review; Table 3 - $CO_2/SO_2 = 2.85 \pm 0.17$; $H_2O/SO_2 = 315 \pm 71.8$; $SO_2/HCl = 1.6 \pm 0.22$).

Date	**05/07/2018**	**06/07/2018**	**07/07/2018**	**08/07/2018**	**09/07/2019**	**Total**
Explosions Counted	8	43	39	36	9	**135**
Data	**05/07/2018**	**06/07/2018**	**07/07/2018**	**08/07/2018**	**09/07/2019**	**Mean**
SO_2 Min (kg)	10.2	8.9	8	12	10	**9.8**
SO_2 Mean (kg)	26.9	22.1	27	39	45	**32.0**
SO_2 Max (kg)	64.1	44.9	62	81	69	**64.2**
Passive %	66	64	70	78	68	**69**
Explosive %	34	36	30	22	32	**31**
Lower Ratios	**05/07/2018**	**06/07/2018**	**07/07/2018**	**08/07/2018**	**09/07/2019**	**Mean**
Total – Min (kg)	712	625	575	822	721	**691**
Total – Mean (kg)	1884	1550	1892	2713	3164	**2241**
Total – Max (kg)	3020	3148	4370	5678	4813	**4206**
Mean Ratios	**05/07/2018**	**06/07/2018**	**07/07/2018**	**08/07/2018**	**09/07/2019**	**Mean**
Total – Min (kg)	940	824	759	1084	952	**912**
Total – Mean (kg)	2486	2046	2497	3579	4175	**2957**
Total – Max (kg)	5929	4153	5767	7493	6350	**5938**
Max Ratios	**05/07/2018**	**06/07/2018**	**07/07/2018**	**08/07/2018**	**09/07/2019**	**Mean**
Total – Min (kg)	1167	1024	942	1347	1182	**1132**
Total – Mean (kg)	3088	2541	3102	4446	5186	**3673**
Total – Max (kg)	7365	5159	7163	9307	7888	**7376**

4.2. Simple Statistical Separation of Passive and Explosive Degassing

Others have looked at the proportions of explosive to passive release during strombolian explosions on Stromboli (Tamburello et al., 2012) and Etna (Pering et al., 2015). Here, we attempt to expand on this by using a simple statistical measure involving the moving minimum, to estimate the passive release of gas through time, which when subtracted from total flux provides an approximate estimate of passive vs. explosive release. On an example period (Figure 7) we highlight the moving minimum, which is set to a window size of 20 s, which is generally the characteristic timeframe of large peaks and troughs associated with strombolian

explosions (Pering et al., 2016). In this instance a moving minimum over this window proved best, given the higher frequency of explosive events, however, with a greater timeframe between events, the moving median may be a better measure. We also prefer this estimation technique over using our estimated SO_2 masses, given that we were selective of strombolian explosions. Commonly this is achieved manually, but simple automated techniques such as this could be valuable in monitoring activity from strombolian explosion producing volcanic systems.

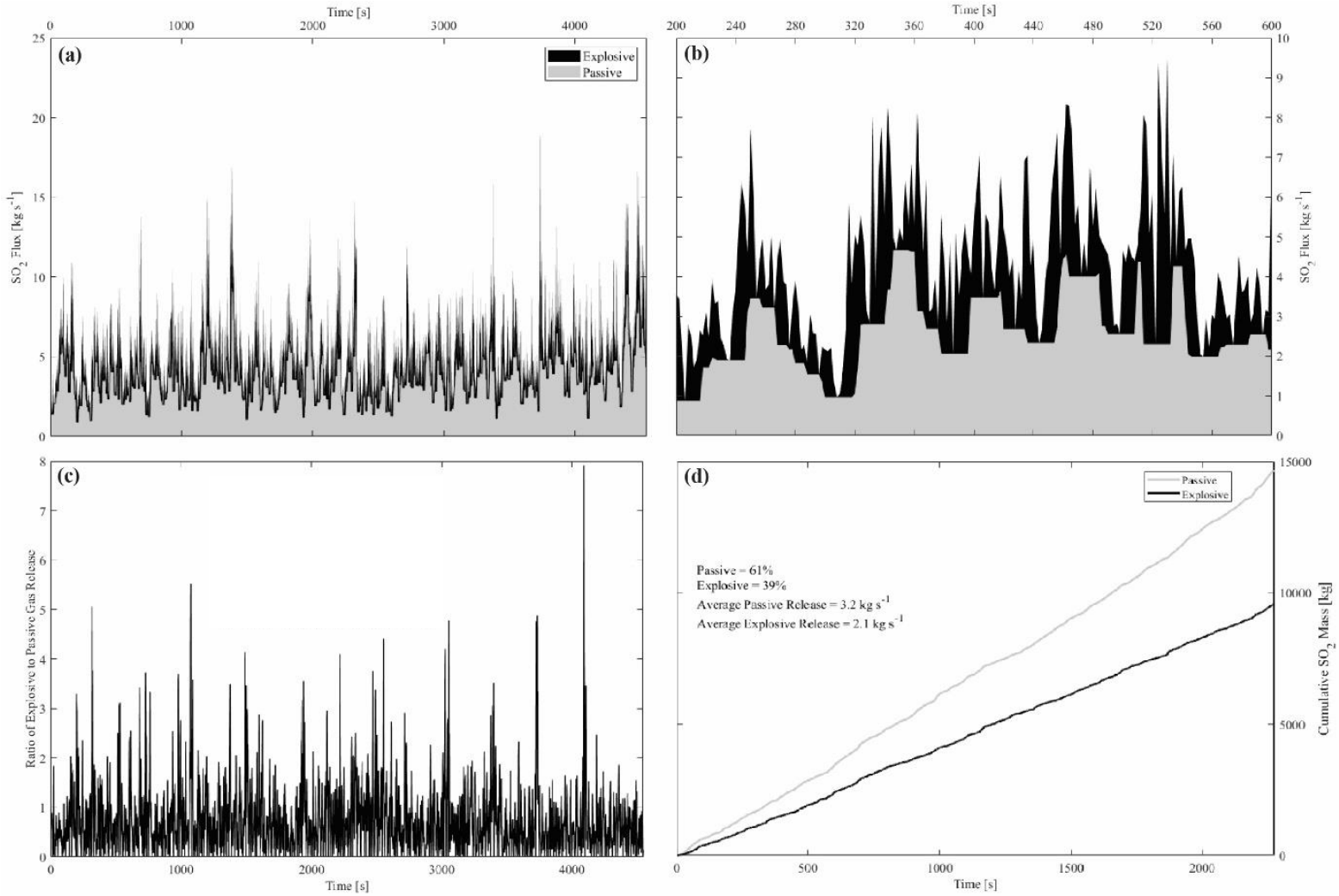

Figure 7: (a) Separation of passive and explosion gas release for a period on the 7th July; (b) a zoomed illustration of the simple statistical model, showing oscillation in background passive degassing overtopped by explosive contributions; (c) the ratio of passive to explosive degassing; and (d) a cumulative plot showing passive and explosive proportioning of gas release.

Day-by-day estimates are detailed in Table 3, with a mean of 69% passive to 31% explosive. These are in line with those measured at Stromboli, 77% passive to 23% explosive (termed active which also includes puffing); and Etna, 67% passive to 33% explosive (Pering et al., 2015). These datasets serve to illustrate the dominant role of passive degassing at volcanoes with strombolian eruptions. On the 8th July we calculated a higher passive contribution at 78%.

At the same time, we measure higher SO_2 masses, but lower overall SO_2 fluxes. This could indicate a magmatic system that is cooling or housing a thickening plug (Polacci et al., 2012; Simons et al., 2020), so becoming less permeable for passive gas release, but also requiring a higher gas mass to drive explosions that may be more powerful, matching our visual observations.

4.3.Models of gas slug behaviour

Using our determined values for total slug mass, we can estimate slug lengths using the static pressure model of (Del Bello et al., 2012). We use fixed values of 2600 kg m^3 and 1000 Pa s^{-1} for density and viscosity, respectively, with an atmospheric pressure of 101,325 Pa. The only parameter we vary in the model is that of conduit diameter, which we step from 3 m to 7 m. We also use only the mean explosive ratios and masses (and not the range obtained when including error) for simplicity. Our results are summarised in Table 4. We determine slug lengths ranging 188 – 609 m (median and mean of 347 m and 366 m respectively) for a conduit diameter of 3 m, however, this reduces to 76 – 260 m (median and mean of 146 and 154 m respectively) for a conduit diameter of 7 m. Kremers et al. (2013) calculated distinctly lower values of 59 – 244 m using seismo-acoustic data, and it would therefore seem that a larger conduit diameter may be more plausible at Yasur, perhaps prior to any conduit bifurcation or splitting at shallow depths (Simons et al., 2020). It should also be noted that the H_2O/SO_2 ratio used in this work are high and variable (Woitischek et al., In Review). As water is the gas contributing most to the mass of the slug, it is likely that our determined masses are an overestimation. In addition, others have shown that UV camera-derived masses can be over-estimated compared with infrasound-derived masses (Dalton et al., 2010).

Table 4: A summary of slug volumes and calculated slug lengths using the model of Del Bello et al. (2012), based on mean ratios for explosive (active) degassing.

Statistic	Slug Volume (m^3)	D = 3 m	D = 4 m	D = 5 m	D = 6 m	D = 7 m
Min	4286	188	139	110	90	76
Median	14055	347	259	205	170	146
Mean	15556	366	272	217	180	154
Max	42337	609	455	364	303	260

5. Summary and Conclusions

In this work we highlighted the utility of using low-cost solar-powered Raspberry Pi UV cameras for prolonged field campaigns. We were able to continuously image the volcanic plume to yield both velocity, using a PIV method (Thielicke, 2014; Thielicke and Stamhuis, 2014), and SO_2 fluxes over periods of several hours per day, at temporal resolutions of up to 0.5 Hz with brief pauses for calibration. Our determined SO_2 fluxes with means 4.1-5.5 kg s^{-1} (medians from 4.0-5.1 kg s^{-1}) are within the ranges of those measured previously using ground based methods of 2.5 to 17.2 kg s^{-1} (Bani et al., 2012; Bani and Lardy, 2007). We further highlight SO_2 masses of strombolian explosions of 8-81 kg, showing these to be of similar to events at Stromboli at 2 – 55 kg (Tamburello et al., 2012). By using a simple statistical measure

we estimate that passive degassing, at 69%, is the dominant mode of degassing at Yasur, compared to 31% explosive. Our brief observation period are suggestive that periods of lower gas output could lead to conduit sealing and more visibility violent explosions, however, a longer dataset would be needed to test this hypothesis substantively. By combining SO_2 explosion masses with gas ratios (Woitischek et al., In Review) we determined total explosion masses of mean ~910-5940 kg, which correspond to slug lengths, using the model of Del Bello et al. (2012) of ~76-260 m, if a larger conduit diameter of ~7 m is used. Smaller conduit diameters lead to far longer slug lengths ~188-600 m at 3 m diameter, larger than those estimated previously of ~59 – 244 m (Kremers et al., 2013).

This work and others (Ilanko et al., 2019) have further highlighted the utility of using a multiple UV camera approach to gas measurements at volcanoes, particularly when thinking about errors of data, and introduced the PIV method for plume flux determination, which we suggest could be robustly used across a variety of plume conditions. The data presented here represent an important addition to our arsenal of gas based information about strombolian style activity globally.

6. Acknowledgements

We would like to thank the Vanuatu Meteorology and Geo-hazards Department for permission to conduct this fieldwork, Kelson and Joyce Hosea for their hospitality at the Jungle Oasis, and Rogar for his assistance in the field. J.W and M.E .were supported by the Natural Environment Research Council (grant number NE/L002507/1), by the postgraduate travel funds received from Fitzwilliam College, by the Elspeth Matthews grant given by the Royal Geological Society, by the Mary Euphrasia Mosley, Sir Bartle Frere and Worts travel fund report given by the University of Cambridge and by the Exzellenzstipendium received by WKO. A.A. acknowledges funding support from the Alfred P. Sloan Foundation via the Deep Carbon Observatory (UniPa-CiW subcontract 10881-1262) and from MIUR (under grant n. PRIN2017-2017LMNLAW). T.D.P. acknowledges the support of the Royal Society (RG170226). T.I. is a Commonwealth Rutherford Fellow, funded by the UK government.

7. References

Aiuppa, A., Coco, E. Lo, Liuzzo, M., Giudice, G., 2016. Terminal Strombolian activity at Etna's central craters during summer 2012: The most CO 2-rich volcanic gas ever recorded at Mount Etna. Geochemical.

Aiuppa, A., Federico, C., Giudice, G., Gurrieri, S., 2005. Chemical mapping of a fumarolic field: La Fossa Crater, Vulcano Island (Aeolian Islands, Italy). Geophys. Res. Lett. 32, L13309. https://doi.org/10.1029/2005GL023207

Bani, P., Lardy, M., 2007. Sulphur dioxide emission rates from Yasur volcano, Vanuatu archipelago. Geophys. Res. Lett. 34. https://doi.org/10.1029/2007GL030411

Bani, P., Oppenheimer, C., Allard, P., Shinohara, H., Tsanev, V., Carn, S., Lardy, M., Garaebiti, E., 2012. First estimate of volcanic SO 2 budget for Vanuatu island arc. J. Volcanol. Geotherm. Res. 211–212, 36–46. https://doi.org/10.1016/j.jvolgeores.2011.10.005

Barnie, T., Bombrun, M., Burton, M.R., Harris, A., Sawyer, G., 2015. Quantification of gas

and solid emissions during Strombolian explosions using simultaneous sulphur dioxide and infrared camera observations. J. Volcanol. Geotherm. Res. 300, 167–174. https://doi.org/10.1016/j.jvolgeores.2014.10.003
Barth, A., Edmonds, M., Woods, A., 2019. Valve-like dynamics of gas flow through a packed crystal mush and cyclic strombolian explosions. Sci. Rep. 9, 821. https://doi.org/10.1038/s41598-018-37013-8
Battaglia, A., Bitetto, M., Aiuppa, A., Rizzo, A.L., Chigna, G., Watson, I.M., D'Aleo, R., Juárez Cacao, F.J., de Moor, M.J., 2018. The Magmatic Gas Signature of Pacaya Volcano, With Implications for the Volcanic CO_2 Flux From Guatemala. Geochemistry, Geophys. Geosystems 19, 667–692. https://doi.org/10.1002/2017GC007238
Blackburn, E.A., Wilson, L., Sparks, R.S.J., 1976. Mechanisms and dynamics of strombolian activity. J. Geol. Soc. London. 132, 429–440. https://doi.org/10.1144/gsjgs.132.4.0429
Branca, S., Del Carlo, P., 2005. Types of eruptions of Etna volcano AD 1670-2003: Implications for short-term eruptive behaviour. Bull. Volcanol. 67, 732–742. https://doi.org/10.1007/s00445-005-0412-z
Burton, M., Allard, P., Mure, F., La Spina, A., 2007. Magmatic Gas Composition Reveals the Source Depth of Slug-Driven Strombolian Explosive Activity. Science (80). 317, 227–230. https://doi.org/10.1126/science.1141900
Campion, R., Delgado-Granados, H., Mori, T., 2015. Image-based correction of the light dilution effect for SO_2 camera measurements. J. Volcanol. Geotherm. Res. 300, 48–57. https://doi.org/10.1016/j.jvolgeores.2015.01.004
Campion, R., Martinez-Cruz, M., Lecocq, T., Caudron, C., Pacheco, J., Pinardi, G., Hermans, C., Carn, S., Bernard, A., 2012. Space and ground-based measurements of sulphur dioxide emissions from Turrialba Volcano (Costa Rica). Bull. Volcanol. 74, 1757–1770. https://doi.org/10.1007/s00445-012-0631-z
Carn, S.A., Fioletov, V.E., Mclinden, C.A., Li, C., Krotkov, N.A., 2017. A decade of global volcanic SO_2 emissions measured from space. Sci. Rep. 7, 1–12. https://doi.org/10.1038/srep44095
Chouet, B., Dawson, P., Ohminato, T., Martini, M., Saccorotti, G., Giudicepietro, F., De Luca, G., Milana, G., Scarpa, R., 2003. Source mechanisms of explosions at Stromboli Volcano, Italy, determined from moment-tensor inversions of very-long-period data. J. Geophys. Res. Solid Earth 108, 2019. https://doi.org/10.1029/2002JB001919
D'Aleo, R., Bitetto, M., Delle Donne, D., Tamburello, G., Battaglia, A., Coltelli, M., Patanè, D., Prestifilippo, M., Sciotto, M., Aiuppa, A., 2016. Spatially resolved SO_2 flux emissions from Mt Etna. Geophys. Res. Lett. 43, 7511–7519. https://doi.org/10.1002/2016GL069938
Dalton, M.P., Waite, G.P., Watson, I.M., Nadeau, P.A., 2010. Multiparameter quantification of gas release during weak Strombolian eruptions at Pacaya Volcano, Guatemala. Geophys. Res. Lett. 37. https://doi.org/10.1029/2010GL042617
Del Bello, E., Llewellin, E.W., Taddeucci, J., Scarlato, P., Lane, S.J., 2012. An analytical model for gas overpressure in slug-driven explosions: Insights into Strombolian volcanic eruptions. J. Geophys. Res. Solid Earth 117. https://doi.org/10.1029/2011JB008747
Delle Donne, D., Ripepe, M., 2012. High-frame rate thermal imagery of strombolian explosions: Implications for explosive and infrasonic source dynamics. J. Geophys. Res. Solid Earth 117, 1–12. https://doi.org/10.1029/2011JB008987
Delle Donne, D., Ripepe, M., Lacanna, G., Tamburello, G., Bitetto, M., Aiuppa, A., 2016. Gas mass derived by infrasound and UV cameras: Implications for mass flow rate. J. Volcanol. Geotherm. Res. 325, 169–178. https://doi.org/10.1016/j.jvolgeores.2016.06.015
Dibble, R.R., Kyle, P.R., Rowe, C.A., 2008. Video and seismic observations of Strombolian

eruptions at Erebus volcano, Antarctica. J. Volcanol. Geotherm. Res. 177, 619–634. https://doi.org/10.1016/j.jvolgeores.2008.07.020
Firth, C.W., Handley, H.K., Cronin, S.J., Turner, S.P., 2014. The eruptive history and chemical stratigraphy of a post-caldera, steady-state volcano: Yasur, Vanuatu. Bull. Volcanol. 76, 1–23. https://doi.org/10.1007/s00445-014-0837-3
Garcés, M.A., Hagerty, M.T., Schwartz, S.Y., 1998. Magma acoustics and time-varying melt properties at Arenal Volcano, Costa Rica. Geophys. Res. Lett. 25, 2293–2296. https://doi.org/10.1029/98GL01511
Gaudin, D., Moroni, M., Taddeucci, J., Scarlato, P., Shindler, L., 2014a. Pyroclast Tracking Velocimetry: A particle tracking velocimetry-based tool for the study of Strombolian explosive eruptions. J. Geophys. Res. Solid Earth 119, 5369–5383. https://doi.org/10.1002/2014JB011095
Gaudin, D., Taddeucci, J., Scarlato, P., del Bello, E., Ricci, T., Orr, T., Houghton, B., Harris, A., Rao, S., Bucci, A., 2017a. Integrating puffing and explosions in a general scheme for Strombolian-style activity. J. Geophys. Res. Solid Earth 122, 1860–1875. https://doi.org/10.1002/2016JB013707
Gaudin, D., Taddeucci, J., Scarlato, P., Harris, A., Bombrun, M., Del Bello, E., Ricci, T., 2017b. Characteristics of puffing activity revealed by ground-based, thermal infrared imaging: the example of Stromboli Volcano (Italy). Bull. Volcanol. 79, 24. https://doi.org/10.1007/s00445-017-1108-x
Gaudin, D., Taddeucci, J., Scarlato, P., Moroni, M., Freda, C., Gaeta, M., Palladino, D.M., 2014b. Pyroclast Tracking Velocimetry illuminates bomb ejection and explosion dynamics at Stromboli (Italy) and Yasur (Vanuatu) volcanoes. J. Geophys. Res. Solid Earth 119, 5384–5397. https://doi.org/10.1002/2014JB011096
Gliß, J., Stebel, K., Kylling, A., Dinger, A., Sihler, H., Sudbø, A., Gliß, J., Stebel, K., Kylling, A., Dinger, A.S., Sihler, H., Sudbø, A., 2017. Pyplis–A Python Software Toolbox for the Analysis of SO_2 Camera Images for Emission Rate Retrievals from Point Sources. Geosciences 7, 134. https://doi.org/10.3390/geosciences7040134
Ilanko, T., Pering, T., Wilkes, T., Apaza Choquehuayta, F., Kern, C., Díaz Moreno, A., De Angelis, S., Layana, S., Rojas, F., Aguilera, F., Vasconez, F., McGonigle, A., 2019. Degassing at Sabancaya volcano measured by UV cameras and the NOVAC network. Volcanica 2, 239–252. https://doi.org/10.30909/vol.02.02.239252
James, M.R., Lane, S.J., Corder, S.B., 2008. Modelling the rapid near-surface expansion of gas slugs in low-viscosity magmas. Geol. Soc. London, Spec. Publ. 307, 147–167. https://doi.org/10.1144/GSL.SP.2003.213.01.17
James, M.R., Lane, S.J., Wilson, L., Corder, S.B., 2009. Degassing at low magma-viscosity volcanoes: Quantifying the transition between passive bubble-burst and Strombolian eruption. J. Volcanol. Geotherm. Res. 180, 81–88. https://doi.org/10.1016/j.jvolgeores.2008.09.002
Jaupart, C., Vergniolle, S., 1989. The generation and collapse of a foam layer at the roof of a basaltic magma chamber. J. Fluid Mech. 203, 347–380. https://doi.org/10.1017/S0022112089001497
Jaupart, C., Vergniolle, S., 1988. Laboratory models of Hawaiian and Strombolian eruptions. Nature 331, 58–60. https://doi.org/10.1038/331058a0
Johnson, J.B., Aster, R.C., 2005. Relative partitioning of acoustic and seismic energy during Strombolian eruptions. J. Volcanol. Geotherm. Res. 148, 334–354. https://doi.org/10.1016/j.jvolgeores.2005.05.002
Johnson, J.B., Ripepe, M., 2011. Volcano infrasound: A review. J. Volcanol. Geotherm. Res. 206, 61–69. https://doi.org/10.1016/J.JVOLGEORES.2011.06.006
Kantzas, E.P., McGonigle, A.J.S., Tamburello, G., Aiuppa, A., Bryant, R.G., 2010. Protocols

for UV camera volcanic SO_2 measurements. J. Volcanol. Geotherm. Res. 194, 55–60. https://doi.org/10.1016/j.jvolgeores.2010.05.003
Kern, C., Lübcke, P., Bobrowski, N., Campion, R., Mori, T., Smekens, J.-F., Stebel, K., Tamburello, G., Burton, M., Platt, U., Prata, F., 2015. Intercomparison of SO_2 camera systems for imaging volcanic gas plumes. J. Volcanol. Geotherm. Res. 300, 22–36. https://doi.org/10.1016/j.jvolgeores.2014.08.026
Kern, C., Sutton, J., Elias, T., Lee, L., Kamibayashi, K., Antolik, L., Werner, C., 2014. An automated SO_2 camera system for continuous, real-time monitoring of gas emissions from Kīlauea Volcano's summit Overlook Crater. J. Volcanol. Geotherm. Res. 300, 81–94. https://doi.org/10.1016/j.jvolgeores.2014.12.004
Kern, C., Werner, C., Elias, T., Sutton, A.J., Lübcke, P., 2013. Applying UV cameras for SO_2 detection to distant or optically thick volcanic plumes. J. Volcanol. Geotherm. Res. 262, 80–89. https://doi.org/10.1016/j.jvolgeores.2013.06.009
Klein, A., Lübcke, P., Bobrowski, N., Kuhn, J., Platt, U., 2017. Plume propagation direction determination with SO_2 cameras. Atmos. Meas. Tech 10, 979–987. https://doi.org/10.5194/amt-10-979-2017
Kremers, S., Wassermann, J., Meier, K., Pelties, C., van Driel, M., Vasseur, J., Hort, M., 2013. Inverting the source mechanism of Strombolian explosions at Mt. Yasur, Vanuatu, using a multi-parameter dataset. J. Volcanol. Geotherm. Res. 262, 104–122. https://doi.org/10.1016/j.jvolgeores.2013.06.007
Laiolo, M., Massimetti, F., Cigolini, C., Ripepe, M., Coppola, D., 2018. Long-term eruptive trends from space-based thermal and SO_2 emissions: a comparative analysis of Stromboli, Batu Tara and Tinakula volcanoes. Bull. Volcanol. 80, 1–19. https://doi.org/10.1007/s00445-018-1242-0
Liu, E.J., Wood, K., Mason, E., Edmonds, M., Aiuppa, A., Giudice, G., Bitetto, M., Francofonte, V., Burrow, S., Richardson, T., Watson, M., Pering, T.D., Wilkes, T.C., McGonigle, A.J.S., Velasquez, G., Melgarejo, C., Bucarey, C., 2019. Dynamics of Outgassing and Plume Transport Revealed by Proximal Unmanned Aerial System (UAS) Measurements at Volcán Villarrica, Chile. Geochemistry, Geophys. Geosystems 20, 730–750. https://doi.org/10.1029/2018GC007692
Lübcke, P., Bobrowski, N., Illing, S., Kern, C., Alvarez Nieves, J.M., Vogel, L., Zielcke, J., Delgado Granados, H., Platt, U., 2013. On the absolute calibration of SO_2 cameras. Atmos. Meas. Tech. 6, 677–696. https://doi.org/10.5194/amt-6-677-2013
Marchetti, E., Ripepe, M., Harris, A.J.L., Delle Donne, D., 2009. Tracing the differences between Vulcanian and Strombolian explosions using infrasonic and thermal radiation energy. Earth Planet. Sci. Lett. 279, 273–281. https://doi.org/10.1016/j.epsl.2009.01.004
McCormick, B.T., Herzog, M., Yang, J., Edmonds, M., Mather, T.A., Carn, S.A., Hidalgo, S., Langmann, B., 2014. A comparison of satellite- and ground-based measurements of SO_2 emissions from tungurahua volcano, Ecuador. J. Geophys. Res. 119, 4264–4285. https://doi.org/10.1002/2013JD019771
McGonigle, A.J.S., Aiuppa, A., Ripepe, M., Kantzas, E.P., Tamburello, G., 2009. Spectroscopic capture of 1 Hz volcanic SO_2 fluxes and integration with volcano geophysical data. Geophys. Res. Lett. 36, 1–5. https://doi.org/10.1029/2009GL040494
McGonigle, A.J.S., Hilton, D.R., Fischer, T.P., Oppenheimer, C., 2005. Plume velocity determination for volcanic SO_2 flux measurements. Geophys. Res. Lett. 32, 1–4. https://doi.org/10.1029/2005GL022470
McGonigle, A.J.S., Pering, T.D., Wilkes, T.C., Tamburello, G., D'Aleo, R., Bitetto, M., Aiuppa, A., Willmott, J.R., 2017. Ultraviolet Imaging of Volcanic Plumes: A New Paradigm in Volcanology. Geosciences 7, 68. https://doi.org/10.3390/geosciences7030068

Meier, K., Hort, M., Wassermann, J., Garaebiti, E., 2016. Strombolian surface activity regimes at Yasur volcano, Vanuatu, as observed by Doppler radar, infrared camera and infrasound. J. Volcanol. Geotherm. Res. 322, 184–195. https://doi.org/10.1016/j.jvolgeores.2015.07.038

Métrich, N., Allard, P., Aiuppa, A., Bani, P., Bertagnini, A., Shinohara, H., Parello, F., Di Muro, A., Garaebiti, E., Belhadj, O., Massare, D., 2011. Magma and Volatile Supply to Post-collapse Volcanism and Block Resurgence in Siwi Caldera (Tanna Island, Vanuatu Arc). J. Petrol. 52, 1077–1105. https://doi.org/10.1093/petrology/egr019

Mori, T., Burton, M., 2009. Quantification of the gas mass emitted during single explosions on Stromboli with the SO_2 imaging camera. J. Volcanol. Geotherm. Res. 188, 395–400. https://doi.org/10.1016/j.jvolgeores.2009.10.005

Oppenheimer, C., Bani, P., Calkins, J.A., Burton, M.R., Sawyer, G.M., 2006. Rapid FTIR sensing of volcanic gases released by Strombolian explosions at Yasur volcano, Vanuatu. Appl. Phys. B 85, 453–460. https://doi.org/10.1007/s00340-006-2353-4

Parfitt, E.A., 2004. A discussion of the mechanisms of explosive basaltic eruptions. J. Volcanol. Geotherm. Res. 134, 77–107. https://doi.org/10.1016/j.jvolgeores.2004.01.002

Patrick, M.R., Harris, A.J.L., Ripepe, M., Dehn, J., Rothery, D.A., Calvari, S., 2007. Strombolian explosive styles and source conditions: Insights from thermal (FLIR) video. Bull. Volcanol. 69, 769–784. https://doi.org/10.1007/s00445-006-0107-0

Pering, T.D., Ilanko, T., Liu, E.J., 2019a. Periodicity in Volcanic Gas Plumes: A Review and Analysis. Geosci. 2019, Vol. 9, Page 394 9, 394. https://doi.org/10.3390/GEOSCIENCES9090394

Pering, T.D., Ilanko, T., Wilkes, T.C., England, R.A., Silcock, S.R., Stanger, L.R., Willmott, J.R., Bryant, R.G., McGonigle, A.J.S., 2019b. A Rapidly Convecting Lava Lake at Masaya Volcano, Nicaragua. Front. Earth Sci. 6, 241. https://doi.org/10.3389/feart.2018.00241

Pering, T.D., McGonigle, A.J.S., 2018. Combining Spherical-Cap and Taylor Bubble Fluid Dynamics with Plume Measurements to Characterize Basaltic Degassing. Geosciences 8, 42. https://doi.org/10.3390/geosciences8020042

Pering, T.D., McGonigle, A.J.S., James, M.R., Capponi, A., Lane, S.J., Tamburello, G., Aiuppa, A., 2017. The dynamics of slug trains in volcanic conduits: Evidence for expansion driven slug coalescence. J. Volcanol. Geotherm. Res. 348, 26–35. https://doi.org/10.1016/J.JVOLGEORES.2017.10.009

Pering, T.D., McGonigle, A.J.S., James, M.R., Tamburello, G., Aiuppa, A., Delle Donne, D., Ripepe, M., 2016. Conduit dynamics and post-explosion degassing on Stromboli: a combined UV camera and numerical modelling treatment. Geophys. Res. Lett. https://doi.org/10.1002/2016GL069001

Pering, T. D., McGonigle, A.J.S., James, M.R., Tamburello, G., Aiuppa, A., Delle Donne, D., Ripepe, M., 2016. Conduit dynamics and post explosion degassing on Stromboli: A combined UV camera and numerical modeling treatment. Geophys. Res. Lett. 43, 5009–5016. https://doi.org/10.1002/2016GL069001

Pering, T.D., Tamburello, G., McGonigle, A.J.S., Aiuppa, A., Cannata, A., Giudice, G., Patanè, D., 2014. High time resolution fluctuations in volcanic carbon dioxide degassing from Mount Etna. J. Volcanol. Geotherm. Res. 270, 115–121. https://doi.org/10.1016/j.jvolgeores.2013.11.014

Pering, T.D., Tamburello, G., McGonigle, A.J.S., Aiuppa, A., James, M.R., Lane, S.J., Sciotto, M., Cannata, A., Patanè, D., 2015. Dynamics of mild strombolian activity on Mt. Etna. J. Volcanol. Geotherm. Res. 300, 103–111. https://doi.org/10.1016/j.jvolgeores.2014.12.013

Peters, N., Hoffmann, A., Barnie, T., Herzog, M., Oppenheimer, C., 2015. Use of motion

estimation algorithms for improved flux measurements using SO_2 cameras. J. Volcanol. Geotherm. Res. 300, 58–69. https://doi.org/10.1016/j.jvolgeores.2014.08.031
Peters, N., Oppenheimer, C., 2018. Plumetrack: Flux calculation software for UV cameras. Comput. Geosci. 118, 86–90. https://doi.org/10.1016/j.cageo.2018.05.014
Polacci, M., Baker, D.R.D., La Rue, Alexandra, Mancini, L., Allard, P., Rue, A La, Mancini, L., 2012. Degassing behaviour of vesiculated basaltic magmas: an example from Ambrym volcano, Vanuatu Arc 233–234, 55–64. https://doi.org/10.1016/J.JVOLGEORES.2012.04.019
Ripepe, M., Harris, A.J.L., Carniel, R., 2002. Thermal, seismic and infrasonic evidences of variable degassing rates at Stromboli volcano. J. Volcanol. Geotherm. Res. 118, 285–297. https://doi.org/10.1016/S0377-0273(02)00298-6
Ripepe, M., Harris, A.J.L., Marchetti, E., 2005. Coupled thermal oscillations in explosive activity at different craters of Stromboli volcano. Geophys. Res. Lett. 32, 1–4. https://doi.org/10.1029/2005GL022711
Ripepe, M., Marchetti, E., 2002. Array tracking of infrasonic sources at Stromboli volcano. Geophys. Res. Lett. 29, 33-1-33–4. https://doi.org/10.1029/2002gl015452
Salvatore, V., Silleni, A., Corneli, D., Taddeucci, J., Palladino, D.M., Sottili, G., Bernini, D., Andronico, D., Cristaldi, A., 2018. Parameterizing multi-vent activity at Stromboli Volcano (Aeolian Islands, Italy). Bull. Volcanol. 80, 64. https://doi.org/10.1007/s00445-018-1239-8
Sawyer, G.M., Salerno, G.G., Le Blond, J.S., Martin, R.S., Spampinato, L., Roberts, T.J., Mather, T.A., Witt, M.L.I., Tsanev, V.I., Oppenheimer, C., 2011. Gas and aerosol emissions from Villarrica volcano, Chile. J. Volcanol. Geotherm. Res. 203, 62–75. https://doi.org/10.1016/j.jvolgeores.2011.04.003
Seyfried, R., Freundt, A., 2000. Experiments on conduit flow and eruption behavior of basaltic volcanic eruptions. J. Geophys. Res. 105, 23727. https://doi.org/10.1029/2000JB900096
Shinohara, H., Ohminato, T., Takeo, M., Tsuji, H., 2015. Monitoring of volcanic gas composition at Asama volcano, Japan, during 2004–2014. J. Volcanol.
Shinohara, H., Witter, J.B., 2005. Volcanic gases emitted during mild Strombolian activity of Villarrica volcano, Chile. Geophys. Res. Lett. 32, L20308. https://doi.org/10.1029/2005GL024131
Simons, B.C., Jolly, A.D., Eccles, J.D., Cronin, S.J., 2020. Spatiotemporal Relationships between Two Closely-spaced Strombolian-style Vents, Yasur, Vanuatu. Geophys. Res. Lett. 47. https://doi.org/10.1029/2019GL085687
Spina, L., Taddeucci, J., Cannata, A., Gresta, S., Lodato, L., Privitera, E., Scarlato, P., Gaeta, M., Gaudin, D., Palladino, D.M., 2016. Explosive volcanic activity at Mt. Yasur: A characterization of the acoustic events (9–12th July 2011). J. Volcanol. Geotherm. Res. 322, 175–183. https://doi.org/10.1016/j.jvolgeores.2015.07.027
Spina, A. La, Burton, M.R., Harig, R., Mure, F., Rusch, P., Jordan, M., Caltabiano, T., 2013. New insights into volcanic processes at Stromboli from Cerberus, a remote-controlled open-path FTIR scanner system. J. Volcanol. Geotherm. Res. 249, 66–76. https://doi.org/10.1016/j.jvolgeores.2012.09.004
Suckale, J., Keller, T., Cashman, K. V, Persson, P.-O., 2016. Flow-to-fracture transition in a volcanic mush plug may govern normal eruptions at Stromboli. Geophys. Res. Lett. 43, 12071–12081. https://doi.org/10.1002/2016GL071501
Sweeney, D., Kyle, P.R., Oppenheimer, C., 2008. Sulfur dioxide emissions and degassing behavior of Erebus volcano, Antarctica. J. Volcanol. Geotherm. Res. 177, 725–733. https://doi.org/10.1016/j.jvolgeores.2008.01.024
Szramek, L., Gardner, J.E., Larsen, J., 2006. Degassing and microlite crystallization of

basaltic andesite magma erupting at Arenal Volcano, Costa Rica. J. Volcanol. Geotherm. Res. 157, 182–201. https://doi.org/10.1016/j.jvolgeores.2006.03.039
Taddeucci, J., Edmonds, M., Houghton, B., James, M.R., Vergniolle, S., 2015. Hawaiian and Strombolian Eruptions, in: The Encyclopedia of Volcanoes. Elsevier, pp. 485–503. https://doi.org/10.1016/b978-0-12-385938-9.00027-4
Taddeucci, J., Scarlato, P., Capponi, A., Del Bello, E., Cimarelli, C., Palladino, D.M., Kueppers, U., Bello, E. Del, Cimarelli, C., Palladino, D.M., Kueppers, U., 2012. High-speed imaging of Strombolian explosions: The ejection velocity of pyroclasts. Geophys. Res. Lett. 39, 1–6. https://doi.org/10.1029/2011GL050404
Tamburello, G., Aiuppa, A., Kantzas, E.P., Mcgonigle, A.J.. S., Ripepe, M., 2012. Passive vs . active degassing modes at an open-vent volcano (Stromboli , Italy). Earth Planet. Sci. Lett. 359–360, 106–116. https://doi.org/10.1016/j.epsl.2012.09.050
Tamburello, G., Aiuppa, A., McGonigle, A.J.S., Allard, P., Cannata, A., Giudice, G., Kantzas, E.P., Pering, T.D., 2013. Periodic volcanic degassing behavior: The Mount Etna example. Geophys. Res. Lett. 40, 4818–4822. https://doi.org/10.1002/grl.50924
Thielicke, W., 2014. The flapping flight of birds : analysis and application. [Thesis].
Thielicke, W., Stamhuis, E.J., 2014. PIVlab – Towards User-friendly, Affordable and Accurate Digital Particle Image Velocimetry in MATLAB. J. Open Res. Softw. 2. https://doi.org/10.5334/jors.bl
Vergniolle, S., Boichu, M., Caplan-Auerbach, J., 2004. Acoustic measurements of the 1999 basaltic eruption of Shishaldin volcano, Alaska 1. Origin of Strombolian activity. J. Volcanol. Geotherm. Res. 137, 109–134. https://doi.org/10.1016/j.jvolgeores.2004.05.003
Vergniolle, S., Jaupart, C., 1986. Separated two-phase flow and basaltic eruptions. J. Geophys. Res. Solid Earth 91, 12842–12860. https://doi.org/10.1029/JB091iB12p12842
Vergniolle, S., Métrich, N., 2016. A bird's eye view of "Understanding volcanoes in the Vanuatu arc." J. Volcanol. Geotherm. Res. https://doi.org/10.1016/j.jvolgeores.2016.08.012
Wilkes, T., McGonigle, A., Pering, T., Taggart, A., White, B., Bryant, R., Willmott, J., 2016. Ultraviolet Imaging with Low Cost Smartphone Sensors: Development and Application of a Raspberry Pi-Based UV Camera. Sensors 16, 1649. https://doi.org/10.3390/s16101649
Wilkes, T., Pering, T., McGonigle, A., Tamburello, G., Willmott, J., 2017. A Low-Cost Smartphone Sensor-Based UV Camera for Volcanic SO_2 Emission Measurements. Remote Sens. 9, 27. https://doi.org/10.3390/rs9010027
Williams-Jones, G., Horton, K.A., Elias, T., Garbeil, H., Mouginis-Mark, P.J., Sutton, A.J., Harris, A.J.L., 2006. Accurately measuring volcanic plume velocity with multiple UV spectrometers. Bull. Volcanol. 68, 328–332. https://doi.org/10.1007/s00445-005-0013-x
Woitischek, J., Woods, A.W., Edmonds, M., Oppenheimer, C., Aiuppa, A., Pering, T.D., Ilanko, T., D'Aleo, R., Garaebiti, E., In Review. Strombolian eruptions and dynamics of magma degassing at Yasur Volcano (Vanuatu). J. Volcanol. Geotherm. Res. In Review